Available online at www.sciencedirect.com
ScienceDirect
EPSL
Earth and Planetary Science Letters xx (2008) xxx–xxx
www.elsevier.com/locate/epsl

Miocene rise of the Shillong Plateau and the beginning of the end for the Eastern Himalaya

Marin K. Clark [a,*], Roger Bilham [b]

[a] Department of Geological Sciences University of Michigan Ann Arbor, MI 48109, USA
[b] Department of Geological Sciences University of Colorado Boulder, CO 80309, USA

Received 2 April 2007; received in revised form 11 January 2008; accepted 22 January 2008

Editor: R.D. van der Hilst

Abstract

A common feature of convergent plate boundaries is the self-organization of strain, exhumation and topography along discrete, arcuate boundaries. Deviations from this geometry can represent first-order changes in stress applied at a plate boundary that must affect how strain is partitioned within the interior of an orogen. The simplicity of the Himalayan fold and thrust belt seen along its central portion breaks down along the eastern extremity of the arc where the 400 km-long Shillong Plateau has developed. This change in strain partitioning affects nearly 25% of the arc and has not previously been considered to be important to the orogen's development. New low-temperature thermochronometry data that suggest this structure initiated in mid to late Miocene time, significantly earlier than was previously estimated from the sedimentary record alone. Development of the Shillong Plateau may be linked to a number of kinematic changes within the Himalayan and Burman collision zones that occur at the same time. These events include the onset of E–W extension in central Tibet, eastward expansion of high topography of the Tibetan Plateau, onset of rotation of crustal fragments in southeastern Tibet, and re-establishment of eastward subduction beneath the Indo-Burman ranges. We suggest that the coincidence of these tectonic events is related to the 'dismemberment' of the eastern Himalayan arc, signifying a change in regional stress applied along the India–Eurasia–Burma plate boundaries. Discrepancies between vertical long-term faulting rates and geodetically derived far-field convergence rates suggest that the collisional boundary in the eastern Himalayan system may be poorly coupled due to introduction of oceanic and transitional crust into the eastern plate boundary. The introduction of dense material into the plate boundary late in the orogen's history may explain regional changes in the strain field that affect not only the Himalaya, but also the deformation field more than 1000 km into the Tibetan Plateau.

Keywords: tectonics; plate boundaries; thermochronology; geomorphology; Himalaya; Tibet

1. Introduction

Understanding the relationship between fold and thrust belt deformation developed at a convergent plate boundary, and the propagation of strain, topography and crustal thickening away from that plate boundary to form an orogenic plateau is a first-order question in continental dynamics. The archetypical example of such is the Himalaya fold and thrust belt and the Tibetan Plateau, which have formed in response to ongoing continental convergence between India and Eurasia. Nearly a third of modern plate convergence is neatly concentrated across a few tens of kilometers in the central Himalaya — a relationship that changes dramatically along strike. In the eastern Himalaya system, strain is more widely distributed. Also, the downgoing plate is composed of transitional and oceanic lithosphere, and the complexity of oblique subduction beneath the Burma micro-plate is introduced. The unique eastern Himalaya system east of 88°E latitude represents nearly 25% of the length of the arc and yet has been poorly considered to be a significant geodynamic influence on the orogen's development.

A dramatic and unique feature of the eastern Himalaya system is the deformation of the Indian foreland basement

* Corresponding author. Tel.: +1 734 615 0484; fax: +1 734 763 4690.
E-mail addresses: marinkc@umich.edu (M.K. Clark), bilham@colorado.edu (R. Bilham).

0012-821X/$ - see front matter © 2008 Published by Elsevier B.V.
doi:10.1016/j.epsl.2008.01.045

beneath the Shillong Plateau. The Shillong Plateau occupies a region between the nearly orthogonal thrust belts of the south-vergent eastern Himalaya and the west-vergent Indo-Burman ranges, which accommodate convergence between India and Eurasia and oblique convergence between India and the Burma micro-plate, respectively (Fig. 1). It is arguably the largest, active basement fold structure in the world, and is 5 to 10 times larger than its commonly-cited analogs found in the Laramide orogeny of the western US or the Sierras Pampeanas of the Andean orogen (Allmendinger et al., 1983; Cross, 1986). Newly available SRTM 90-meter resolution digital topography data of the Shillong Plateau show a smooth, regular erosion surface that defines a doubling-plunging, south-vergent anticline composed of Proterozoic and Archean basement rocks in the core of the range and dipping Cretaceous to Miocene(?) age sedimentary rocks on the limbs (Fig. 2). The crest of this anticline is flat-topped, giving rise to the moniker 'Shillong Plateau'. Archean and Neoproterozoic granites and gneisses of the peninsular Indian shield are exposed along most of the central and northern portions of the anticline, while up to 6 km of Cretaceous through Miocene, marine to continental sedimentary rocks are preserved unconformably over basement along the eastern, western and southern limbs (Evans, 1964; Das Gupta et al., 1964; Das Gupta and Biswas, 2000; Ghosh et al., 2005) (Fig. 1). The orientation of these sedimentary rocks generally follows the overall topographic trend of the anticline, except in the south where normal displacements occur locally within the Cenozoic strata (Srinivasan, 2005). Rocks of the Shillong Plateau over thrust shelf to basinal facies sedimentary rocks of the Sylhet Trough (Bengal Basin) to the south (Das Gupta et al., 1964) (Fig. 1).

We interpret the anticlinal folding of sedimentary strata and exposure of the basement core to be the result of a blind or emergent reverse fault system at depth (Fig. 1). The existence of thrust or reverse faults beneath the Shillong Plateau is supported by gravity data and compressional earthquake focal mechanisms (Verma and Mukhopadhyay, 1977; Chen and Molnar, 1990; Mitra et al., 2005), although the sense of motion along the southern bounding fault of the Shillong Plateau (Dauki Fault) has been controversial (Oldham, 1854; Oldham, 1899; Evans, 1964; Hiller and Elahi, 1984; Johnson and Alam, 1991; Biham and England, 2001; Srinivasan, 2005). Modeling of triangulation data following the 1897 Assam earthquake suggests that the northern edge of the Shillong Plateau is controlled by a steeply dipping fault that penetrates most, if not all of the crust, and mirrors motion on the steeply dipping Dauki Fault to the south (Chen and Molnar, 1990; Biham and England, 2001). A seismogenic lower crust is supported by deep diffuse seismicity (Kayal et al., 2006) and steep bounding faults are a geometry that is commonly observed in analogous basement compressional structures in many other orogens (Narr and Suppe, 1994). Digital topography shows that the exposed basement rocks are intensely fractured and that rivers are deeply incised only in their lower reaches along the southern boundary, and along a

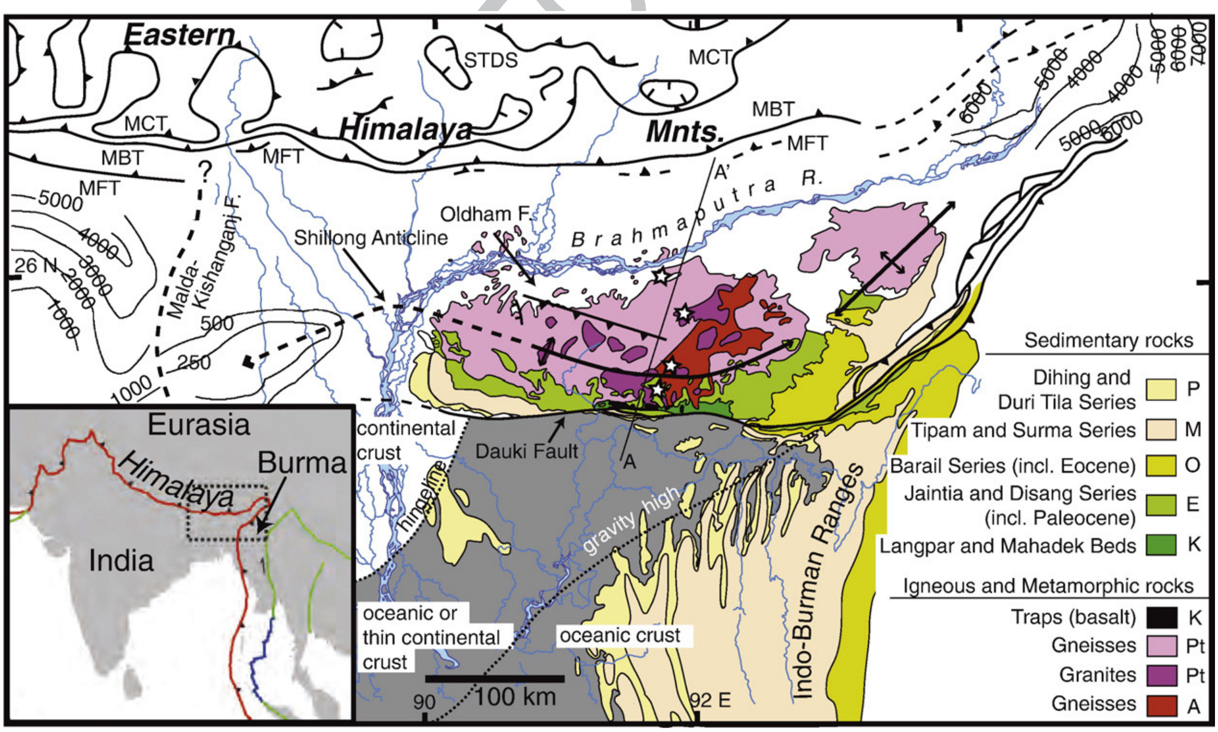

Fig. 1. Geological map of the Shillong Plateau and surrounding region. (U-Th-Sm)/He sample locations (stars) where southernmost sample location is a vertical transect (Table 1). Abbreviations: MFT, Main Frontal Fault; MBT, Main Boundary Thrust; MCT, Main Central Thrust; STDS, South Tibetan Detachment System. Thick lines represent faults and fold axes. Thin lines west and east of the plateau represent isopach depth contours (m) of Himalayan foredeep. Map sources (Das Gupta et al., 1964; Chowdhury, 1973; Biham and England, 2001, India, 2002; Srinivasan, 2005; Hollister and Grujic, 2006; Robinson, 2006) and this study. Inset map shows location of major and micro plates relevant to this study. Red, green and blue lines represent convergent, transform, and divergent plate boundaries. (For interpretation of the references to colour in this figure legend, the reader is referred to the web version of this article.)

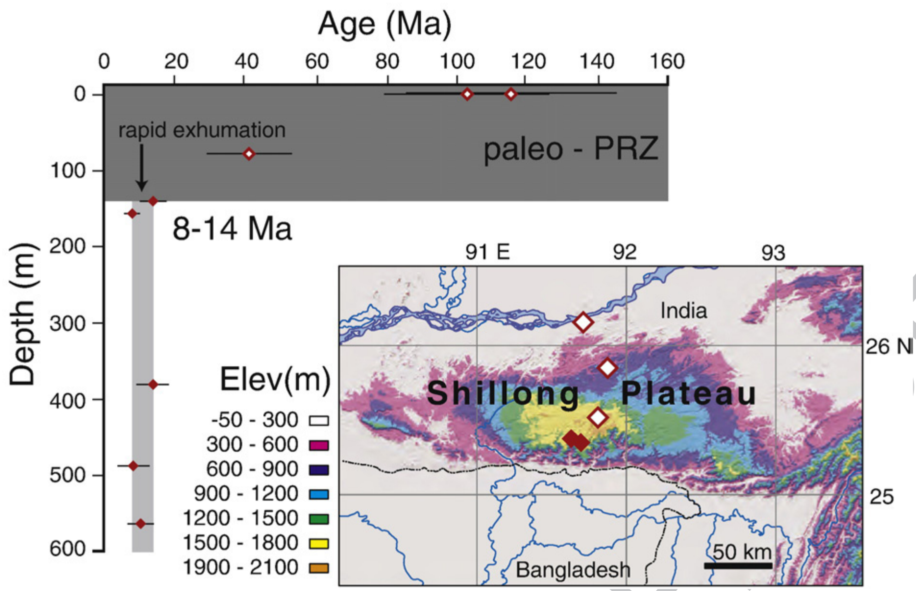

Fig. 2. (U-Th-Sm)/He age/depth plot and sample map with digital topography. Open diamond symbols represent samples collected along a horizontal N–S transect. Solid symbols represent vertical (elevation) transect collected in river gorge. Sample ages are mean ages and error bars represent 2σ standard error of single-grained replicate analyses (Table A1).

west-northwest trending topographic step within the northern limb of the anticline. While some south-draining river canyons reach 1.5 km deep, incision is limited to short, downstream reaches of the major rivers and the landscape overall is not extensively dissected. Lack of fluvial dissection preserves the basement/cover unconformity that defines the surface of the basement fold.

Shortening strain in the eastern Himalaya is widely distributed over several hundred kilometers and includes basement rocks of the underthrust plate (India), whereas strain in the western and central Himalaya occurs in a more narrowly focused manner across a few tens of kilometers and rarely more than 100 km (Das Gupta et al., 1964; Gansser, 1983; Bilham et al., 1997; Lave and Avouac, 2000; Wobus et al., 2005). Recently measured GPS velocities suggest that possibly as much as 30% of the 15–19 mm/yr of convergence across the eastern Himalayan system occurs across the Shillong Plateau (Biham and England, 2001; Jade et al., 2004). Furthermore, approximately 30% of the Tibetan Plateau (~30%) sits north of the eastern Himalaya and adjacent India/Burma plate boundary. Understanding eastward expansion of the Tibetan Plateau may in part depend on understanding how changes at the plate boundary affect strain distribution far within the orogen. Deformation of the Shillong Plateau signals differentiation of the eastern Himalaya from the rest of the Himalaya and a regionally-significant change in how strain is partitioned at the plate boundary. Therefore the timing of Shillong deformation can be used to assess the relationship between deformation at the plate boundary (Himalaya) and the interior of the orogen (Tibetan Plateau).

2. Timing of deformation and tectonic interpretation from basinal stratigraphy: summary of previous work

Previous estimates for timing of fault motion beneath the Shillong Plateau are based on the sedimentary record of the Sylhet Trough (or Surma Basin), a province of the larger Bengal Basin. These estimates vary considerably from the Oligocene–Miocene boundary to Pliocene time. Basinal strata are also preserved along the up-thrust margins of the Shillong massif itself. However, tectonic interpretation of basinal stratigraphy is hampered by multiple sources of tectonic loading and sediment supply (Himalaya, Shillong Plateau, and the Indo-Burman Ranges) as well as uncertainties in the age designation of Neogene units. Sedimentary rocks reach thicknesses up to 16–17 km in the Bengal Basin and thin northward to 4–5 km on the southern Shillong Plateau. Sequences consist of late Mesozoic and Cenozoic shallow marine, continental shelf and deltaic facies that grade upward to fluvial/floodplain deposits of late Miocene or Pliocene age (e.g., Evans, 1964; Hiller and Elahi, 1984; Brune and Singh, 1986; Johnson and Alam, 1991; Uddin and Lundberg, 1998a,b; Alam et al., 2003). The oldest sedimentary rocks suggest that the southern boundary of the Shillong Plateau initiated as a rift margin in early Cretaceous time (Curray et al., 1982; Salt et al., 1986). Sedimentation continued in a passive-margin setting throughout Palaeocene and Eocene time, and is represented by a shelf to basin transgressive sedimentary sequence followed by a regressive sequence of prograding shelf and slope sediments by Late Eocene time after the India–Eurasia collision commenced (Banerji, 1981; Rao Ranga, 1983; Rowley, 1996).

Some workers regard the mid-Eocene transgression as the earliest signal of foreland subsidence in response to Himalaya thrusting because of the coincidental timing between transgression and hard-collision of India with Eurasia (Alam et al., 2003), while others suggest that Himalayan influence in the sedimentary record of the Sylhet trough does not begin until possibly Oligocene, and probably not until early Miocene time based on sandstone petrology and heavy mineral suites (Uddin and Lundberg, 1998a,b, 2004) or detrital mica $^{40}Ar/^{39}Ar$

thermochronology (Rahman and Faupl, 2003). A more likely dominant tectonic influence on basin sedimentation during Oligocene to Miocene time is the encroachment of the Indo-Burman ranges from the east, which is supported by the eastward thickening of sedimentary units and the greater proximity of the Bengal Basin to the Indo-Burman ranges than the Himalaya during this time (Johnson and Alam, 1991; Uddin and Lundberg, 2004).

Alam et al. (2003) suggested that the marine transgression in the Bengal Basin at the Oligocene–Miocene boundary represents flexural loading in response to fault motion on the Dauki Fault and the rise of the Shillong Plateau. However, Oligocene and Miocene age rocks do not thicken northward in the Sylhet Trough as might be expected if the Shillong Plateau initiated flexural subsidence during this time (Johnson and Alam, 1991). During late Miocene to Pliocene time, the upward transition from the prodelta-deltaic sequences of the marine Surma Group to the fluvial non-marine Tipam group, with an accompanying dramatic increase in sedimentation rate and northward thickening of sedimentary strata, has also been regarded as the initial timing of flexural loading and subsidence due to thrust faulting along the Dauki Fault (Johnson and Alam, 1991). However, age designations of the Surma to Tipam group transition as identified by a regional stratigraphic marker (Upper Marine Shales) vary considerably from ~11 Ma to as young as 4 Ma (Johnson and Alam, 1991; Uddin and Lundberg, 1998a,b; Worm et al., 1998; Alam et al., 2003). These sequences lack precise age dating by radiometric ages or age-indicative fossils and instead rely on lithostratigraphic correlation with other locations in India, magentostratigraphic sections lacking independent age constraints, and unpublished, oil-industry palynological reports (Evans, 1932; Rao Ranga, 1983; Banerji, 1984; Hiller and Elahi, 1984; Johnson and Alam, 1991; Reimann, 1993; Uddin and Lundberg, 1998a,b; Worm et al., 1998; Alam et al., 2003; Uddin and Lundberg, 2004).

Uncertainties in stratigraphic age designations and multiple sources of detritus limit our ability to interpret the timing of fault motion beneath the Shillong Plateau from the sedimentary record to broadly Oligocene–Pliocene time. Such broad age estimates hamper our ability to relate deformation of the Shillong Plateau with other regional tectonic events, or to produce geologic faulting rates spanning less than an order of magnitude. Cooling histories derived from thermochronometry data may provide an unambiguous measure of tectonic activity and a more precise age estimate of faulting than the stratigraphic record alone.

3. Timing of deformation from apatite (U-Th-Sm)/He thermochronometry

Samples collected for low-temperature thermochronometry along horizontal and vertical transects can give information about the spatial distribution of erosion and timing of erosional events related to structural activity. We collected 14 samples for apatite (U-Th-Sm)/He dating along a north–south horizontal transect across the central plateau and a vertical transect within a single river gorge that incises the southern margin of the plateau (Figs. 1 and 2). We aim to determine the thickness of paleo-sedimentary cover and subsequent erosion of the plateau surface and the timing of initial fault motion from accelerated erosion rates related to vertical motion across a reverse fault. Samples were collected from Neoproterozoic granites and granitic gneisses (Ghosh et al., 2005) and 4 to 11 single-grained replicate analyzes were measured for each sample depending on apatite yield and quality, which varied between samples (Tables 1 and A1). Sample preparation and analytical methods are described in Appendix A.

Four samples were collected at or within 150 m depth below the plateau surface from the most northern exposure of bedrock in the Brahmaputra valley to the southern edge of the anticlinal crest. These ages vary systematically both from north to south and with increasing depth from 115.7 to 13.9 Ma (Fig. 2; Table 1). Six samples collected above and within a narrow river gorge on the southern limb of the anticline (including sample 04Sh3 which overlaps the two transects) have mean ages clustered between 13.9 and 8 Ma (Table 1) excluding Sample 04Sh5, which reproduced poorly compared to other samples and is not included in Fig. 2 (Table A1). While the mean ages do not systematically decrease in age, as may be theoretically expected in response to erosional exhumation, the narrow range of helium ages and overlap of replicate ages suggests that rapid exhumation initiated within this time interval. In particular, the change from broadly distributed mean ages within 150 m depth of the plateau surface to a narrow age range at greater depth is also suggestive of accelerated cooling rates associated with increased exhumation focused at the southern plateau margin.

Table 1
Sample locations and mean (U-Th-Sm)/He ages

Sample	Latitude (°N)	Longitude (°E)	Elevation (m)	Lithology	Mean age (Ma±2σ)	No. replicates
04SH3	25.3722	91.6349	1558	Porphyritic granite	13.9±3.6	8
04SH4	25.3433	91.6997	1543	Granite	8.0±2.0	4
04SH5	25.3452	91.7008	1450	Granite	22.5±15.6	8
04SH6	25.3475	91.7004	1318	Granite	13.9±4.6	11
04SH7	25.3492	91.6999	1211	Granite	8.1±4.2	4
04SH8	25.3517	91.6994	1137	Granite	10.1±3.6	7
04SH9a	25.5179	91.8127	1721	Granite	40.4±12.2	6
04SH10	25.8478	91.8777	574	Granitic gneiss	103.2±23.2	4
04SH13	26.1625	91.7130	93	Granitic gneiss	115.7±29.6	4

Please cite this article as: Clark, M.K., Bilham, R., Miocene rise of the Shillong Plateau and the beginning of the end for the Eastern Himalaya, Earth Planet. Sci. Lett. (2008), doi:10.1016/j.epsl.2008.01.045

We regard the age range of 14 to 8 Ma to best represent the possible range of initial of rapid cooling.

The broad age range at shallow intervals is typical of samples that spent a long residence time in the partial retention zone and were either closed or partially closed to helium diffusion during a later exhumation event that exposes them at the surface today. The change from a broad age range to a narrow age range with respect to depth (i.e. a change from slow or no cooling to rapid cooling) represents the depth of the base of the partial retention zone (PRZ) at the time of the onset of rapid cooling. Using a closure temperature based on a model of radiation damage and cooling rate (60 °C) (Schuster et al., 2006), the exposure of a paleo-PRZ also represents a paleodepth estimate of 1.7–3.3 km at the time of closure to helium diffusion for a range of typical continental geothermal gradients (15–30 °C and surface temperature 10 °C). A paleo-PRZ depth of ~150 m beneath the modern plateau surface suggests that 1.7–3.3 km of overburden must have existed above our transect at the time of initiation of rapid exhumation and has been removed since fault activity began. This overburden is likely to have been Mesozoic to Cenozoic age sedimentary rocks that once capped the central plateau and are still preserved on the southern and lateral flanks of the plateau. Our estimate of overburden is less than the 4–6 km of sediment preserved on the flanks of the plateau (Johnson and Alam, 1991). This discrepancy may reflect variations in the sediment thickness across the plateau, or uncertainty in the geothermal gradient or closure temperature. Estimates of the amount of eroded overburden above the central plateau are used to calculate vertical fault motion in Section 6.

Determination of long-term fault slip rates requires an understanding of the fault geometry at depth, which has been controversial (Srinivasan, 2005; Chen and Molnar, 1990; Biham and England, 2001; Seeber and Armbruster, 1981; Rajendran et al., 2004; Biham). In the next section, we examine geomorphic data as evidence of active faulting patterns.

4. Geomorphology and fluvial analyzes

Bedrock river channel gradients are sensitive indicators of variable rock uplift rates in an actively deforming region and can be used qualitatively to identify faulting patterns. This approach can be particularly useful in remote areas, areas of dense vegetative cover, or where the lack of appropriate aged rocks involved in recent deformation inhibit determination of young or active faulting. We utilized the method outlined by Kirby et al. (2003) for determining normalized steepness values for channel segments based on a stream-power law for bedrock erosion and the hydrologic processing methods given by Niemi and Oskin (2004). These methods employ a commonly-used, empirical scaling law that relates local channel slope (S) of a river to the contributing drainage area (A) at that channel segment, where drainage area is a proxy for discharge through the channel parameters of steepness (k_s) and concavity (θ) (e.g., Flint, 1974):

$$S = k_s A^{-\theta}, \tag{1}$$

Using a reference concavity value ($\theta_{\rm ref}$), we calculate quantified normalized steepness values ($k_{\rm sn}$) of stream segments to identify regions of high steepness that may indicate increased relative rock uplift rates due to reverse faulting across proposed structures. Channel slope and drainage area data were extracted from a hydrologically-corrected, 90-m resolution DEM (STRM data) in order to calculate

$$k_{\rm sn} = SA^{\theta},\ \text{for reference}\ \theta_{\rm ref} = 0.45. \tag{2}$$

Using hydrologic routing, channel pixels with contributing drainage area greater than a threshold value of 0.1 km^2 were selected then divided into 0.5 km channel segments over which channel slope was averaged by a least squares fit to the elevation profile of the channel segment. Using Eq. (2), normalized channel steepness was determined for each channel pixel from the average channel slope for a segment centered on that pixel and the contributing drainage area to that pixel. Data noise was reduced by eliminating segments with poor slope regressions ($R^2<0.5$) and negative or zero slope values.

Normalized channel steepness values range from 1 to 5600, although most values are <100 (Fig. 3). Values >700 occur in isolation, over a single channel segment, and are likely caused by data artifacts, such as artificial steps in the DEM created during processing or data dropout, jointing/boulder cascades creating stepped profile segments, non-bedrock channel erosion processes especially in headwater regions (low drainage area regions), or other transient erosion processes occurring at or near knickpoints or knickzones. Because a contrast in lithology can also affect the steepness values due to differences in erodibility, we only consider values within the basement core of the anticline and neglect consideration of the lateral flanks of the plateau where significant sedimentary cover is still present (Fig. 1). For stream values with drainage area >40 km^2, the highest consistent $k_{\rm sn}$ values that occur over several channel segments is 500 in deeply incised streams along the southern and northeastern plateau boundaries, and up to 700 in streams incised into the hanging wall block of the proposed Oldham fault.

We interpret high steepness values in the south to reflect higher vertical motion along the steep limb of the anticline and/or to channel segments that are in a transient phase adjusting to south-vergent folding. Most major south-draining channel segments contain abrupt knickpoints or knickzones that separate lower gradient headwater portions within the fold axis with much steeper gradients on downstream portions of channels draining the steep, south-facing limb of the anticline above the Dauki Fault. Deep channel incision and canyon-cutting into bedrock of up to 1500 m depth occurs only downstream of major knickpoints. The pattern of high steepness values along the southern plateau margin does not discriminate between a model where a steep anticline develops above a blind thrust fault, or whether the Dauki Fault must project to the surface. There is an obvious pattern of high steepness values oriented along the proposed surface projection of the Oldham Fault that does not correlate with a lithologic change or variation in jointing. We interpret these high steepness values as confirmation of the

Please cite this article as: Clark, M.K., Bilham, R., Miocene rise of the Shillong Plateau and the beginning of the end for the Eastern Himalaya, Earth Planet. Sci. Lett. (2008), doi:10.1016/j.epsl.2008.01.045

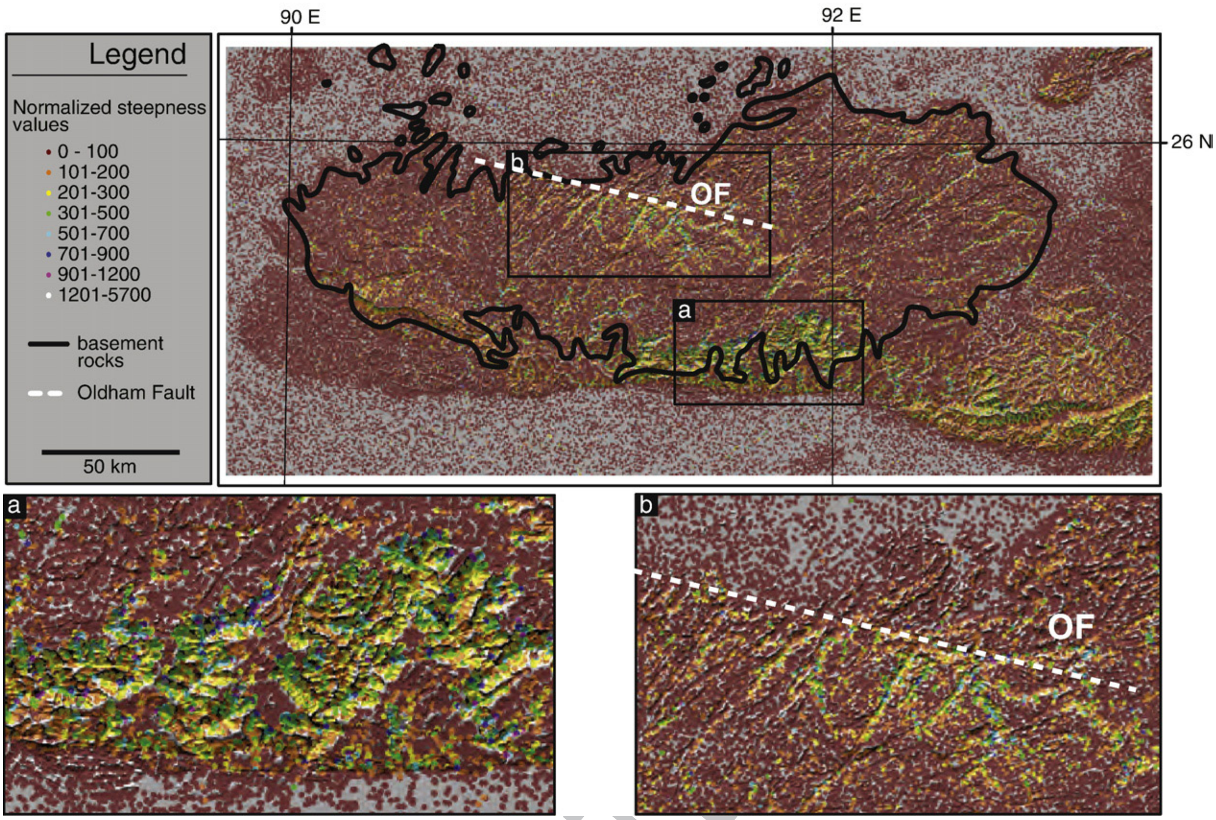

Fig. 3. Map of normalized steepness values draped on shaded relief map of the Shillong Plateau. Black outline is the extent of Proterozoic and Archean basement granites and gneisses from Fig. 1. White dashed line (OF) is the surface projection of the Oldham Fault(Biham and England, 2001). a) Close-up view of heavily dissected southern range. b) Close-up of Oldham Fault region.

orientation and activity of the Oldham Fault as proposed by Bilham and England (Biham and England, 2001), contrary to the suggested lack of surface fault expression argued by Rajendran et al. (2004).

5. Constraints on structural geometry beneath plateau

The spatial extent of deformation associated with the Shillong Plateau can be estimated from both the extent of exposed basement and sedimentary rocks and the limit of missing or attenuated foredeep deposits surrounding the plateau (Fig. 1). Thin foredeep deposits exist west of the Shillong Plateau to the Malda-Kishanganj Fault where they abruptly deepen from 500 m to several kilometers across this structure (India, 2002). Northeast of the Shillong Plateau, the foredeep eventually deepens to 4–6 km about 100 km northeast of the exposed basement and elevated topography of the Mirkir Hills (India, 2002) (Fig. 1). Isolated basement outcrops within the Brahmaputra valley are evident from field observations and digital topography maps and suggest that sedimentary deposits are unusually thin (a few to several hundred meters) for at least 50 km north of the Shillong Plateau (India, 2002; Rajendran et al., 2004). The exact thickness of sedimentary deposits proximal to the Himalayan range front north of the Shillong Plateau is unknown, but is estimated to be not more than 1 km thick based on gravity values and the width of the Himalayan foredeep is no more than 30 km wide (Mathur and Evans, 1964) whereas it is 200 km wide in Nepal. Himalayan foredeep sediments are exposed in Bhutan in the hanging wall of the Main Frontal Thrust (MFT). A homoclinally, north-dipping section of fluvial sandstones and conglomerates suggest that at least 6 km of foredeep sediments were deposited proximal to the Himalaya prior to deformation of the MFT (Gansser, 1983)(N. Mc Quarrie, pers. comm.). A precise stratigraphic age of these sediments has not been determined, but are likely correlative with the Upper Miocene to Pleistocene Silwalk Group in Nepal and Pakistan [N. Mc Quarrie, pers. comm.].

The interpretation of triangulation data from the 1897 Assam earthquake suggests that the Oldham Fault ruptured on a steeply dipping plane from between 9 km to at least 25 km, and possibly the entire crust (Biham and England, 2001) (Fig. 4). This constraint requires that the Dauki Fault must also be steeply dipping. However, we suggest that the Oldham fault is not a bounding structure to the Shillong Plateau, as in a pop-up structure. It does not form the northern topographic boundary of the plateau, but rather forms a small topographic step that is largely within the plateau itself and causes only a minor offset in the largely anticlinal geometry of the plateau (Figs. 2 and 4). Most importantly, Himalayan foredeep rocks present east and west of the Shillong Plateau are missing beneath the Brahmaputra valley, directly north of the Oldham Fault and the plateau itself (Fig. 1). This requires that a structural block beneath the Brahmaputra

Please cite this article as: Clark, M.K., Bilham, R., Miocene rise of the Shillong Plateau and the beginning of the end for the Eastern Himalaya, Earth Planet. Sci. Lett. (2008), doi:10.1016/j.epsl.2008.01.045

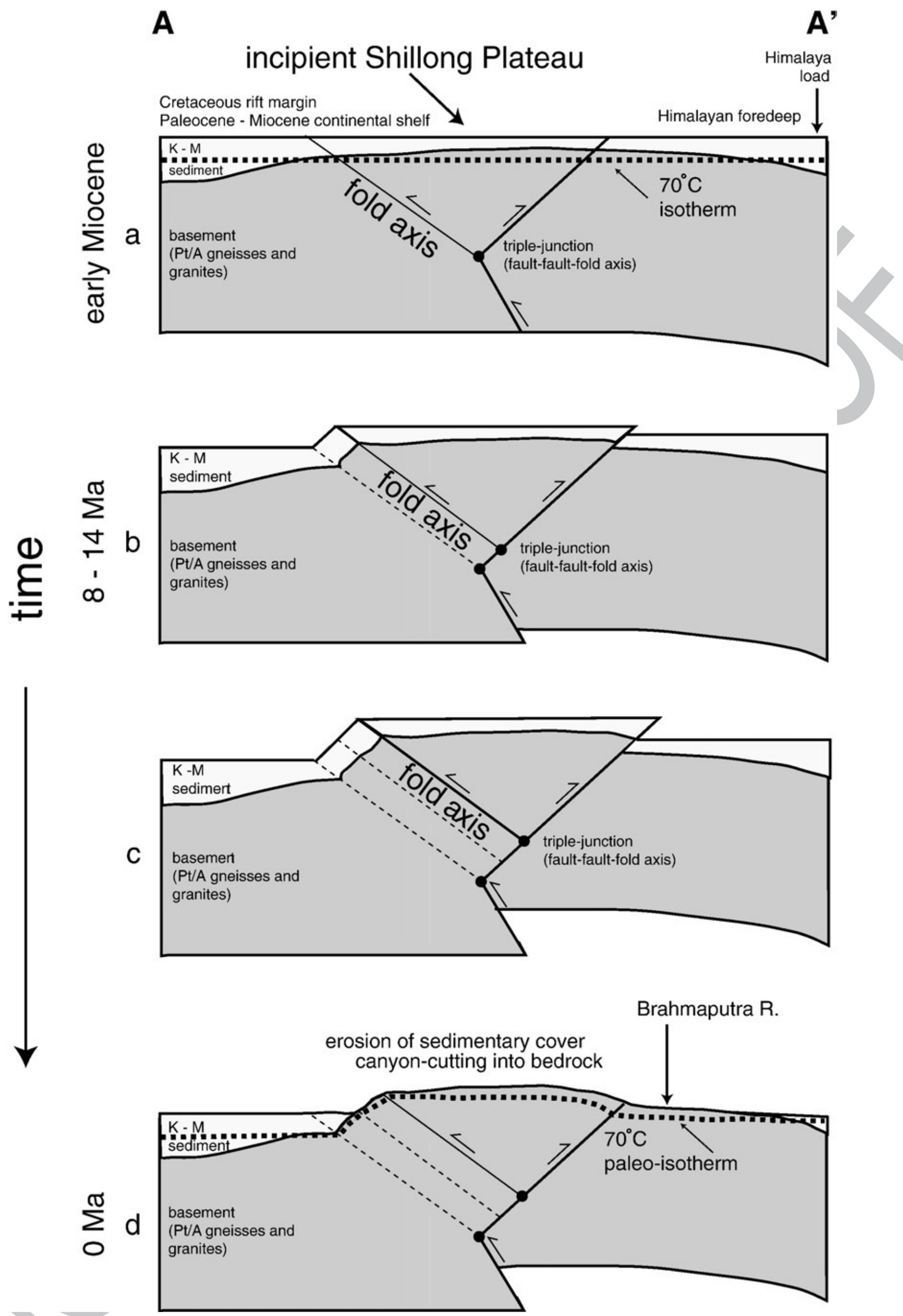

Fig. 4. Hypothesized structural evolution of the Shillong Plateau. North on right. (a) Initial fault geometry at fault inception. Based on helium cooling ages, ~2–3 km of sedimentary rocks covered the central Shillong Plateau. Thick dashed line represents the position of the PRZ at the timing of fault initiation. (b) and (c) Motion on a master deep fault at depth initiates folding of basement rocks above the southern boundary and development of a steep backthrust to the north. Progressive upward motion likely initiates broad removal of easily eroded sedimentary cover over basement rocks. (d) Present-day geometry. Sedimentary rocks have been stripped above the central plateau. Thick dashed line represents modern position of the paleo-PRZ formed at the time of fault (fold) initiation.

valley also have moved upward causing the erosion of foredeep sediments.

We propose that the Oldham Fault is a backthrust to a master, blind, north-dipping fault at depth where a block beneath the Brahmaputra valley acts as the primary hanging wall and a structural wedge develops to form the Shillong Plateau (Fig. 5). We base our proposed geometry on geometric models for commonly occurring basement structures that best fit our structural observations and existing geophysical data (Narr and Suppe, 1994) (Fig. 5). In this model, the surface feature that has been mapped as the Dauki Fault is a fold axis propagating from a blind fault at depth instead of an emergent structure (Fig. 5). Our fault geometry is constrained by the dip of the Oldham Fault (Biham and England, 2001), the depth of the Oldham Fault (Biham and England, 2001), the dip of the south flank of the plateau surface, and the width of the flat-topped portion of the central plateau. A structural block at depth underlies the Brahmaputra valley and moves upward relative to a block

Please cite this article as: Clark, M.K., Bilham, R., Miocene rise of the Shillong Plateau and the beginning of the end for the Eastern Himalaya, Earth Planet. Sci. Lett. (2008), doi:10.1016/j.epsl.2008.01.045

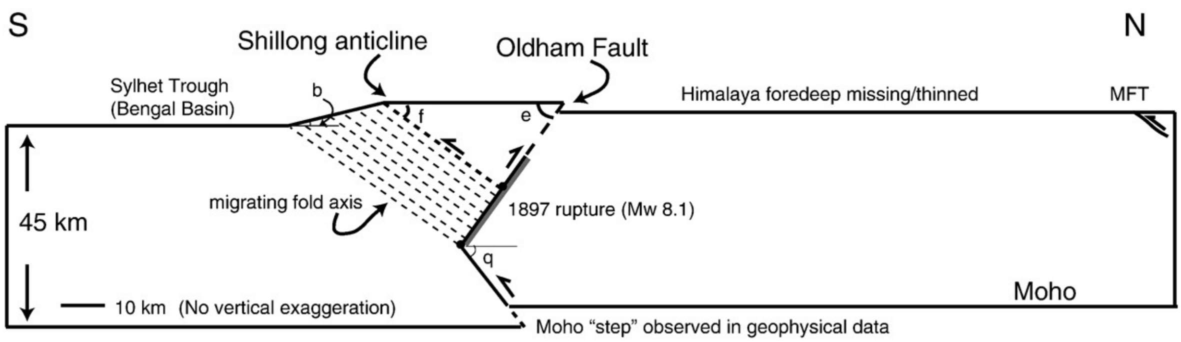

Fig. 5. Proposed structural geometry for the Shillong Plateau. Model angles b, f, and e are constrained by dip of the Oldham Fault (57° Biham and England, 2001), depth of Oldham Fault (30 km (Biham and England, 2001), dip of the south flank of plateau surface (15°), and width of the flat-topped portion of the central plateau surface (60 km). Dip on the master fault at depth (q) is calculated from the model angles (Narr and Suppe, 1994, Eq. (7)).

beneath the Sylhet Trough (Bengal Basin). Upward motion of the Brahmaputra valley causes erosional removal of Himalayan foredeep sediments and produces a step in the Moho that is consistent with the geophysical data (Verma and Mukhopadhyay, 1977; Mitra et al., 2005). The master fault bifurcates at depth into a north-dipping fold axis and a south-dipping backthrust. The fold axis migrates north in time as the structure grows. Using the constraints above, we calculate a dip of 53° for the master fault at depth. Alternatively, the Dauki Fault is emergent and breaks through the entire crust, but does not link kinematically with the Oldham Fault. In this scenario, the Dauki Fault must dip at least 35° in order to obey the geometry of an Oldham Fault extending to depths of 30 km (Biham and England, 2001). Also additional faults must exist beneath the Brahmaputra valley to accommodate its vertical motion. However, there is no surface expression of these faults in the morphology or gravity field of the Brahmaputra valley.

6. Initiation of faulting, fault slip rate and erosion rate

In a compressional tectonic setting, an increase in apparent exhumation rate on an age/elevation diagram is generally assumed to be an acceleration of erosion rate related to the upward motion of hanging wall rocks (Wagner and Reimer, 1972; Wagner et al., 1977; Fitzgerald et al., 1995; Reiners and Brandon, 2006). Using both thermochronometry data and the stratigraphy of the Sylhet Trough, we consider the initiation of faulting, faulting rates and erosion rates independently. Three aspects of the age-elevation diagram are useful to constrain timing of fault initiation, fault slip rate, and erosion rate following fault initiation respectively: (1) a change in exhumation rate, (2) the depth of the paleo-PRZ, and (3) the age-elevation slope of rapidly cooled samples or the helium age at mean elevation. Determination of these ages and rates requires the following assumptions.

(1) We assume that the change in exhumation rate at between 8 and 14 Ma represents the age of fault initiation. This assumption implies that faulting beneath the Shillong Plateau must have produced enough topographic relief under an erosive climate regime such that accelerated erosion rates occurred immediately after faulting began. This assumption may be invalid if initial relief changes were small, if minimally-erosive climate conditions existed at the time of faulting, or if the geologic setting suggests that faulting is not commensurate with sub-aerial exposure, such as a marine setting. If any of the assumptions are invalidated by one of the aforementioned conditions, then the timing of accelerated erosion represents a minimum age of faulting because accelerated erosion rates may have lagged behind fault initiation. Rapid cooling beginning between 8 and 14 Ma is contemporaneous with a Miocene age marine transgression (Upper Marine Shales of the Surma Group) followed by a Miocene to Pliocene (?) age to a northward thickening sequence of continental fluvial-deltaic sandstones (Tipam Group), and an acceleration in subsidence rate in the Sylhet Trough (Hiller and Elahi, 1984; Johnson and Alam, 1991; Reimann, 1993; Worm et al., 1998; Alam et al., 2003; Rahman and Faupl, 2003). The marine to continental transition, geometry and rate of continental deposition in the foredeep south of the Shillong Plateau have been suggested to be related to fault initiation (Johnson and Alam, 1991) with an upper age limit for this stratigraphic transition at 11 Ma (Hiller and Elahi, 1984; Johnson and Alam, 1991; Reimann, 1993; Worm et al., 1998; Alam et al., 2003; Rahman and Faupl, 2003). Therefore we suggest that accelerated erosion rates of the Shillong Plateau can be temporally associated with flexural loading in the Sylhet Trough due to faulting and sub-aerial exposure of the hanging wall rocks evident by the marine to continental change in sedimentary depositional environment.
Modern heavy orographic precipitation occurs across the Himalaya foreland (Anders et al., 2006) and because high relief of the Himalaya reasonably existed during Miocene time, minimally-erosive climate conditions that may have forestalled an acceleration in erosion rates are unlikely.
(2) Whereas we assume that fault initiation triggers an acceleration of erosion rate, it is not necessary to assume that the ensuing erosion rate is equivalent to the vertical fault slip rate. In fact, we *expect* that the long-term

Please cite this article as: Clark, M.K., Bilham, R., Miocene rise of the Shillong Plateau and the beginning of the end for the Eastern Himalaya, Earth Planet. Sci. Lett. (2008), doi:10.1016/j.epsl.2008.01.045

vertical fault slip rate has outpaced erosion because up to 2 km of topography has been created since deposition of marine strata in Miocene time (upper Surma Group). We independently determine the long-term fault slip rate using the base of the paleo-PRZ as a passive marker to vertical deformation. To determine fault slip rate, we establish the offset of a reference horizon in both fault blocks, in this case the offset of the 8–14 Ma land surface across the Dauki Fault (Fig. 6). We use the base of the paleo-PRZ to reconstruct the land surface of the hanging wall at 3.3–4.9 km modern elevation by assuming a geothermal gradient (15–30 °C/km) and closure temperature (60 °C) (Fig. 6). Sedimentary evidence suggests that the transition from the Surma to the Tipam Group likely represents the interval of faulting (Johnson and Alam, 1991). We use the base of the northward thickening Tipam Group sediments at 6 km depth below sea level in the Sylhet Trough (Johnson and Alam, 1991) as the 8–14 Ma land surface in the footwall. Offset between these two surfaces (fault throw) since 8–14 Ma gives a long-term average vertical fault slip rate of 0.7–1.4 mm/yr (Fig. 6). It is important to note that this fault slip rate is faster than the 'rock uplift' rate (cf. Molnar and England, 1990) because the latter only considers motion of the hanging wall block and neglects the downward motion of the footwall block.

(3) Erosion rate is typically determined from the slope of rapidly cooled samples on the age-elevation diagram (Wagner and Reimer, 1972; Wagner et al., 1977; Fitzgerald et al., 1995; Reiners and Brandon, 2006). Neglecting the effect of advection, which is small in cases of moderate or slow exhumation rates, and the horizontal spacing between samples on a 'vertical' transect (e.g. Moore and E.P.C., 2001; Ehlers and Farley, 2003), which was minimal due to our sampling strategy, the apparent exhumation rate is a measure of the long-term erosion rate. An average erosion rate can also be compared to a steady erosion rate based on the depth of the modern closure isotherm versus the helium age at the mean elevation of the landscape (Reiners and Brandon, 2006) or a 'zero age intercept' concept where the age-elevation erosion rate is projected to a 'zero age' and compared to the modern depth of the closure isotherm (Parrish, 1983; Farley et al., 2001). Comparison of steady erosion rates to the erosion rate defined by the sample transect evaluates whether erosion rates determine from the age-elevation plot can be extrapolated to the present. We calculate an average (steady) erosion rate (cf. Reiners and Brandon, 2006) of 0.1–0.4 mm/yr based on a closure temperature of 60 °C (Farley, 2002; Schuster et al., 2006), a range of geothermal gradient between 15 and 30 °C/km, a surface temperature of 10 °C, and an average age of 8–14 Ma. Scatter of single-grain age measurements in the Shillong data prohibit a meaningful regression through the mean age/elevation data however the steady rate of 0.1–0.4 mm/yr is consistent with the age data (Fig. 2).

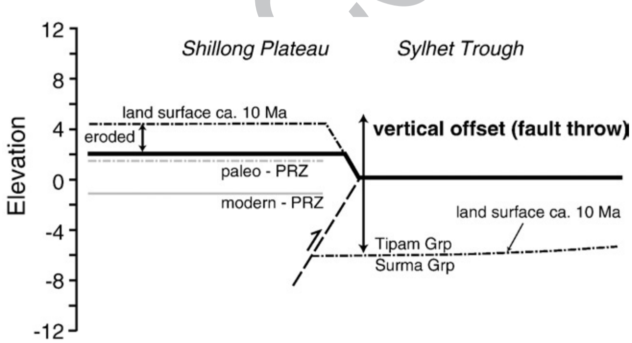

Fig. 6. Diagram of offset markers used to calculate fault slip and erosion rates. Thick black line represents modern topography. Dot-dashed black line represents the median reconstructed land surface of the Shillong Plateau based on the position of the paleo-PRZ (hanging wall) and the beginning of fault related foredeep deposition in the Sylhet Trough (footwall). Vertical offset of these two horizons is fault throw since 8–14 Ma. Offset between paleo-PRZ (dot-dashed grey line) and the modern PRZ (solid grey line) since 8–14 Ma is used to calculate erosion rate.

We call particular attention to the fact that the vertical slip rate (0.7–1.3 mm/yr) is greater than the average erosion rate (0.1–0.4 mm/yr) by at least a factor of two despite the extreme precipitation that falls on the Shillong Plateau (avg. 6 m/yr). In fact, the south-central plateau touts its fame as the 'rainiest place on earth' where precipitation can average 12 m/yr! (Bookhagen et al., 2005) Furthermore, a strong monsoon climate since at least 7–8 Ma (e.g. Kroon, 1991; Prell et al., 1992; Dettman et al., 2001; An et al.) causes a strong seasonality to the distribution of rainfall, which creates intense summer rain storms in Shillong. Despite what might be considered the most extreme erosive conditions imaginable, erosion has not kept pace with faulting over approximately the last 10 million years.

7. Comparison of long-term fault slip rates with geodetic rates

Using our proposed fault geometry (Fig. 5) and vertical slip rates determined above, we calculate the horizontal shortening rate across the Shillong Plateau to be 1.0–2.0 mm/yr. Use of a shallower dip for the Oldham Fault (35°) produces higher horizontal shortening rates of about 1.5–2.9 mm/yr; however, lower rates are obtained if the geodetically determined fault dip of 57°±8° for the Oldham Fault prevails also in the Dauki system (Biham and England, 2001) (Fig. 5).

Faulting rates determined here are at least half of previously determined fault rates based on a Pliocene age of fault initiation derived from the stratigraphic record, and are in poor agreement with published GPS velocities (6±6 mm/yr, Biham and England, 2001) and (4.3±4.8 mm/yr, Jade et al., 2004). However, recent GPS measurements show that Shillong's convergence with India lies at the lower bound of these estimates (3±1 mm/yr, [W. Szeliga, personal communication 2007]), in good agreement with our uplift rates. It is important to note that our helium results record vertical uplift rates, while the GPS data measure horizontal convergence. The two rates are linked by the subsurface geometry of faults beneath the Shillong Plateau and in principle the two rates can be used to constrain this geometry. The calculation, however, requires us to assume that the

Please cite this article as: Clark, M.K., Bilham, R., Miocene rise of the Shillong Plateau and the beginning of the end for the Eastern Himalaya, Earth Planet. Sci. Lett. (2008), doi:10.1016/j.epsl.2008.01.045

present day active structures are similar to the time-averaged structures responsible for the helium uplift rates, and that viscous processes associated with the 1897 earthquake are negligible. A consideration of these effects is outside the scope of the present article.

We propose that the geomorphic evidence for the Oldham fault, together with modeling of triangulation data following the 1897 Assam earthquake for fault geometry (Biham and England, 2001) requires that the faults beneath the Shillong Plateau be steeply dipping. Steeply dipping faults yield calculated horizontal shortening rates near the lower bound of current GPS uncertainties.

8. Discussion

Altogether, we consider the area deforming around the Shillong Plateau to encompass a region nearly 600 km eastward by 150 km northward (90,000 km ^{2}), which accounts for more than 25% of the entire length of the Himalayan arc. We argue that deformation encompasses not only the region of elevated, exposed basement of the Shillong Plateau proper, but also includes deformation of a much larger region of the foreland where Himalayan foredeep rocks are attenuated or missing (Fig. 1). The western extent of the attenuated Himalayan foredeep at the Malda-Kishanganj Fault occurs at about 88°E longitude, which is spatially coincident with other structural changes within the Himalaya and southern Tibet. From west to east across this boundary, a dramatic decrease occurs in the extent of exposed Lesser Himalayan rocks in structural windows or re-entrants; klippen of Tethyan Sedimentary Series bounded by the South Tibetan Detachment System (STDS) suddenly appear, and both the STDS and MCT and are located at least 100 km further south than observed in the west; and the Main Frontal Thrust (MFT) essentially disappears or is poorly exposed (Gansser, 1983). Within southern Tibet, this boundary coincides with the Yadong-Gulu rift system at ~88°E, the most prominent rift system within southern Tibet that accommodates east–west extension within the High Himalaya and southern plateau. The Yadong-Gulu rift forms the boundary between east and west extension within central Tibet and strike-slip systems of eastern Tibet.

The scale of the Shillong Plateau has long been considered to signify a massive departure from the simple Himalayan thrust systems found elsewhere along the arc (Seeber and Armbruster, 1981). These authors were the first to propose a decollement underlying the Brahmaputra valley. The partitioned convergence we describe is manifest as a departure from the small-circle geometry of the Himalaya established by the collision process (Seeber and Gornitz, 1983; Bendick and Biham, 2001), and there is no question that the partitioned convergence between Bhutan and Shillong reduces the seismic productivity of Bhutan. The development of the Shillong structure relatively recently in the collision process suggests that the eastern Himalaya, at least, is evolving into something different than the rest of the arc. Our discussion below focuses on the timing and rate of this process. The question arises, however, whether the process signifies the beginning of the end for the Himalaya, or whether the plateau is a non-propagating structure formed by conditions unique to the eastern end of the arc. If the Shillong plateau evolves will the load shedding potential of the plateau increase or diminish? There is some suggestion of increased development of the plateau to the east, with uplift decaying westward, but this could be the result of counter-clockwise rotation of Assam. No doubt future GPS measurements will determine the underlying motions needed to guide speculation on this important process.

The shallow sedimentary cover in the Brahmaputra Valley north of the plateau, and the absence of a wide foreland basin south of Bhutan, may indicate the presence of additional dip slip faults north of the Oldham fault or vertical motion of a hanging wall block to the Dauki Fault at depth. Alternatively, it is possible that the crustal scale faults of the Shillong system have fractured the northeast Indian plate sufficiently to inhibit long-wavelength (>500 km) plate flexure south of the eastern Himalaya (W.A.B., 2001; Biham et al., 2003). In the central Himalaya, the bending moment load of the southern edge of the Tibetan Plateau and the forces of Indo-Asian convergence give rise to a 4–6 km deep trough near the frontal thrusts of the Himalaya, and a ~600 m high bulge underlying the central Indian plateau. Although the gravity field permits a narrow foreland basin, no outer-rise is manifest at the longitudes of the Shillong Plateau. Such a model explains the lack of subsidence and deposition in the Brahmaputra valley only since deformation at Shillong began. An additional mechanism by which an older foredeep deposits (>10 Ma) would be removed or absent is still required.

Deformation of the Shillong Plateau is also temporally coincident with several major changes in regional strain patterns within the southern Tibetan Plateau and along its eastern margin: onset of graben style extension in south-central Tibet at 18–5 Ma (Pan and Kidd, 1992; Coleman and Hodges, 1995; Williams et al., 2001); eastward expansion of high topography in southeastern Tibet at ~9–13 Ma (Clark et al., 2005) and east-central Tibet at ~5–12 Ma (Kirby et al., 2002); initiation of clockwise rotation of crustal fragments around the eastern syntaxis at 4–8 Ma (Wang et al., 1998); and re-establishment of eastward subduction beneath the Indo-Burman ranges (Mitchell, 1993). Deformation of Silwalk equivalent rocks above the MFT (N. Mc Quarrie, pers. comm.), late Miocene monazite ages in the MCT at approximately 89°E latitude in Sikkim (Catlos et al., 2004), and deformation beneath Shillong suggest possible synchronous faulting of the MCT, MFT and Dauki fault in the eastern Himalaya since about 10 Ma.

The current discrepancy between the long-term horizontal faulting rate derived from uplift (1–3 mm/yr) and recent geodetic convergence rates (3–5 mm/yr) is an outstanding issue worth further exploration. Currently the two numbers can be reconciled only by invoking an unreasonably shallow dip to the Oldham and Daki faults (<40°), or the possible effects of residual high afterslip rates associated with the 1897 Shillong and Dhubri 1930 earthquakes. Convergence is currently partitioned between Shillong and Bhutan in the ratio 1:n where n is 4±1, a ratio that will become more clear in the next decade as more GPS data become available. However, the surface

Please cite this article as: Clark, M.K., Bilham, R., Miocene rise of the Shillong Plateau and the beginning of the end for the Eastern Himalaya, Earth Planet. Sci. Lett. (2008), doi:10.1016/j.epsl.2008.01.045

convergence velocity fields of Bhutan and Shillong overlap in the Brahmaputra Valley and northern Shillong plateau. Thus even in the presence of much improved signal-to-noise GPS velocities, the precise determination of the slip partitioning at depth will remain ambiguous.

It is also possible that poor coupling between the underthrust plate and the structures of the Shillong Plateau may prevail. If the horizontal motion of the underthrust plate is only partially transferred to the overriding plate, then one may expect the horizontal and vertical faulting rates to be less in the Shillong Plateau than otherwise predicted based on the far-field geodetic convergence rate. Although poor coupling in this manner may require modification of the structural geometry we propose. One explanation for the lack of coupling beneath the Shillong Plateau is the subduction of oceanic to transitional crust (Fig. 1). The rheologic contrast of dense crust in the downgoing plate and light continental crust in the overriding plate may be responsible for the lack of complete coupling at this boundary and may explain the discrepancy between high far-field horizontal shortening rates determined by GPS and much slower near-field vertical uplift rates interpreted from thermochronology. Subduction of oceanic and transitional crust is unique to the eastern plate boundary, and most likely, ultimately explains why the eastern portion of the arc deforms differently from the central and western arc.

Deformation of the Shillong Plateau represents a change in the strain distribution of the eastern Himalaya fold and thrust belt indicated by widening the region of active thrusting to several hundred kilometers (Seeber and Armbruster, 1981). At the same time, thrusting in the central Himalaya remains generally concentrated over a few tens of kilometers. The mid-late Miocene change in strain partitioning in the eastern Himalaya possibly explains the deceleration in erosion rates interpreted from fission-track data in Bhutan without need to call upon climatically driven changes suggested by Grujic et al. (2006). Faulting localized at the southern boundary of the Shillong Plateau occurs at the site of a paleo-rift margin that juxtaposes normal thickness continental crust to the north with attenuated continental crust and oceanic crust to the south (Fig. 1). We propose that these changes may be related to the proximity of transitional to oceanic crust at the main plate boundary, caused by the continual northward motion of the Indian plate, which reactivates a paleo-rift margin along the southern boundary of the Shillong Plateau. Furthermore, we suggest that this change from a continent–continent to continent–oceanic (or transitional) plate boundary over a significant region of the Himalayan system initiates a change in the stress field at the plateau boundary which is reflected by changes to the strain field more than 1000 km interior to the orogen.

9. Conclusions

New apatite (U-Th-Sm)/He data suggest deformation of the Shillong Plateau initiated in mid- to late-Miocene time, significantly earlier than was previously estimated from the sedimentary record alone. Helium ages collected within 150 m depth from the plateau surface vary systematically with depth between 116 and 14 Ma and are suggestive of slow cooling during this time interval. Samples collected on a vertical transect along the southern limb of the anticline indicate a change to rapid cooling between 14 and 8 Ma, which we associate with the initiation of fold growth and faulting at depth. Geomorphic and fluvial analyzes used to qualitatively assess the fault geometry beneath the Shillong Plateau suggest steeply dipping faults. Fault geometry, combined with vertical fault offset and timing of fault initiation from our helium data, allow us to estimate a geologically-averaged horizontal and vertical faulting rates of 1.0–2.0 and 0.7–1.4 mm/yr respectively.

Our analysis of high resolution digital topographic data suggests that the underlying geometry driving uplift of the plateau is a south verging fold. Steepened channels in streams flowing north from the apex of this fold confirm the location, strike and sense of slip of the geodetically-inferred subsurface south-dipping Oldham fault, however, despite hosting the $M_w = 8.1$ 1897 'Great Assam' earthquake, the fault appears to be associated with limited cumulative slip. Symmetrical uplift of the Shillong Plateau invoking a pair of conjugate faults (Biham and England, 2001) is thus too simple a model to explain the initiation and rise of the plateau.

Deformation of the Shillong Plateau represents a change in the Himalayan strain partitioning by widening the zone of convergence along the eastern Himalayan plate boundary. New timing constraints for fold initiation given by cooling histories suggests that deformation of the Shillong Plateau may be temporally linked to a number of kinematic changes within the Himalayan and Tibetan orogen, as well as along the eastern India–Burma plate boundary. These events include the onset of E–W extension in central Tibet, eastward expansion of high topography of the Tibetan Plateau, onset of rotation of crustal fragments in southeastern Tibet, and re-establishment of eastward subduction beneath the Indo-Burman ranges. We hypothesize that these mid-late Miocene structural differences in the eastern Himalaya and development of new faults and topography growth in eastern Tibet occur because of a change in the stress state on the collisional plate boundary. We suggest that initiation of faulting beneath the Shillong Plateau moved the plate boundary southward such that transitional and oceanic lithosphere underthrust beneath the Shillong Plateau entered the main collision zone. The change in strain partitioning by fault initiation beneath the Shillong Plateau 'dismembered' the eastern Himalayan arc by southward propagation of faulting into the 'downgoing' Indian plate, which changed the location of the main plate boundary between continental and transitional/oceanic lithosphere. We posit that this fundamental change in lithospheric type at the plate boundary initiated a series of other kinematic changes affecting deformation in regions more than 1000 km interior to the orogen.

Acknowledgments

We thank Ken Farley for access to the Caltech Noble Gas Facility in order to produce our helium measurements. We also thank Anjan Battacharyya, Sanjeev Bhattacharyya, B. P. Durah, Nicole Feldl, Vinod Gaur, Malay Mukul, and C. P.

Rajendran for their assistance during our field work. Ken Farley, Peter Molnar, Karl Mueller, and Nathan Niemi contributed in the valuable discussions regarding helium age reproducibility, structural geometries applicable to the Shillong Plateau and comparisons between geologic and geodetically determined fault slip rates. We also thank Joseph Curray, Sam Johnson, and Ashraf Uddin for their discussions on regional stratigraphy and tectonics. Nadine Mc Quarrie generously provided a generalized map of major Himalayan structures for Fig. 1. Peter Reiners and Nadine McQuarrie gave constructive reviews that helped focus and strengthen arguments put forward in this manuscript. This work was supported by NSF grant EAR0003449 to RB and a Texaco Prize Postdoctoral Fellowship from the California Institute of Technology to MKC.

Appendix A. (U-Th)/He sample preparation and analytical techniques

Apatite separates for (U-Th)/He analyzes were produced from Neoproterozoic granitoids and gneisses (Ghosh et al., 2005) collected during a field campaign 2004 in Meghalaya, India (Table 1). Grains were initially selected for euhedral morphology and scanned for visible inclusions of potentially high U or Th-rich phases under a ~120× binocular microscope using cross-polars. Prior to analysis, grains were measured for the alpha-ejection correction (Farley et al., 1996; Farley, 2000).

Helium outgassing was performed by laser heating procedures (House et al., 1999; House et al., 2000). After outgassing, grains were retrieved, dissolved and spiked with ^{235}U and ^{230}Th and analyzed in a Finnigan Element inductively couple plasma mass spectrometer (ICPMS). All replicate data for a given sample are single-grain analyzes. The number of grains available for each sample varied with the amount and quality of apatite (Table A1). We attempted to run at least 8 replicate analyzes, but some samples did not yield sufficient quality material for more than four replicate analyzes.

Mean ages are reported as the average of replicate analyzes (Table 1). Propagated errors on He ages based on the analytical uncertainty in U, Th, and He measurements are 4% (2σ) for laser samples (Farley, 2000), however we report a 6% (2σ) uncertainty for all replicate ages based on the reproducibility of laboratory standards (Farley, 2002). Mean errors are reported at 2σ as standard errors using the standard deviation of the replicate analyzes divided by $(n-1)$ where n is the number of replicate analyzes performed (Table 1). This uncertainty estimate is much larger than the analytical error alone and is intended to reflect the age grain-to-grain age variability that is typically observed to greater or lesser degree in all samples (Clark and Farley, in press). In general, age variability is greater for single-grain replicate analyzes compared to multi-grain replicate aliquots of previous studies that average several to tens of grains.

Table A1
(U-Th-Sm)/He analytical data

Sample Replicate	U (ppm)	Th (ppm)	He (nmol/g)	Mass (μg)	Radius (μm)	Length (μm)	F_t	Sm (ppm)	Raw age (Ma)	Corrected age[a] (Ma ± 2σ)
04Sh3a	33	112	3.95	4.87	51	343	0.74	555	12.2	16.3 ± 1.0
04Sh3b	10	34	0.75	5.41	57	309	0.76	261	7.5	9.7 ± 0.6
04Sh3c	23	57	2.27	7.79	69	309	0.79	372	11.5	14.5 ± 0.9
04Sh3d	11	26	0.76	7.55	66	326	0.79	171	8.3	10.5 ± 0.6
04Sh3e	17	49	1.36	7.81	57	446	0.77	323	8.8	11.4 ± 0.7
04Sh3f	22	65	1.20	4.81	57	274	0.76	393	5.9	7.8 ± 0.5
04Sh3g	10	27	1.30	3.91	57	223	0.75	142	15.0	20 ± 1.2
04Sh3h	12	30	1.72	8.22	69	326	0.80	194	16.5	20.8 ± 1.2
04Sh4a	31	117	1.39	3.34	51	235	0.73	647	4.3	5.9 ± 0.4
04Sh4b	38	150	3.8	4.78	62	228	0.76	826	7.6	9.9 ± 0.6
04Sh4c	8	36	0.52	4.5	55	254	0.74	465	5.6	7.5 ± 0.5
04Sh4d	72	148	3.94	5.64	56	333	0.76	983	6.7	8.8 ± 0.5
04Sh5a	41	170	3.16	5.11	57	291	0.76	952	7.1	9.3 ± 0.6
04Sh5b	8	31	2.56	6.18	63	291	0.77	421	30.7	38 ± 2.3
04Sh5d	11	40	2.44	2.47	51	174	0.71	360	21.1	29.2 ± 1.8
04Sh5e	13	56	1.86	3.89	55	238	0.74	427	12.8	17.1 ± 1.0
04Sh5f	24	90	1.81	6.84	58	376	0.77	489	7.2	9.4 ± 0.6
04Sh5g	23	75	11.65	3.29	54	209	0.73	591	52.0	70.2 ± 4.2
04Sh5h	10	42	1.31	3.17	53	210	0.73	369	11.7	15.9 ± 1.0
04Sh5i	52	197	15.25	3.27	49	249	0.72	756	28.1	38.8 ± 2.4
04Sh6a	35	163	5.47	3.90	51	274	0.73	852	13.8	18.5 ± 1.1
04Sh6d	46	213	8.52	4.7	54	257	0.74	679	16.3	22 ± 1.3
04Sh6e	37	144	2.38	7.79	69	309	0.79	722	6.1	7.7 ± 0.5
04Sh6f	26	92	3.59	9.45	68	375	0.80	568	13.7	17.1 ± 1.0
04Sh6g[b]	21	90	23.52	2.8	46	179	0.69	441	100.5	143.9 ± 8.6
04Sh6h	54	280	3.91	4.75	66	204	0.77	1236	5.9	7.7 ± 0.5
04Sh6i	41	191	1.92	3.48	48	285	0.72	807	4.1	5.6 ± 0.3
04Sh6j[b]	29	130	12.49	3.82	46	330	0.72	695	37.8	52.5 ± 3.2
04Sh6k	29	136	3.99	3.91	53	258	0.74	701	11.9	16.1 ± 1.0
04Sh6l	27	92	4.8	2.80	50	208	0.72	569	15.3	21.2 ± 1.3

Table A1 (*continued*)

Sample	U	Th	He	Mass	Radius	Length	F_t	Sm	Raw age	Corrected age[a]
Replicate	(ppm)	(ppm)	(nmol/g)	(µg)	(µm)	(µm)		(ppm)	(Ma)	(Ma±2σ)
04Sh6m	36	152	2.60	4.0	52	278	0.73	661	6.6	9±0.5
04Sh7b	16	54	0.77	3.80	54	240	0.74	384	4.9	6.5±0.4
04Sh7c	40	182	3.10	9.85	64	452	0.79	804	6.8	8.6±0.5
04Sh7d	11	38	0.39	9.2	68	362	0.80	425	3.5	4.3±0.3
04Sh7e	8	30	0.89	8.38	64	380	0.79	364	10.3	13±0.8
04Sh8a	4	14	0.34	6.1	57	343	0.76	179	8.4	10.6±0.6
04Sh8b	34	125	4.89	7.51	57	429	0.77	710	14.3	18.3±1.1
04Sh8c	35	155	1.47	2.65	40	309	0.68	679	3.8	5.6±0.3
04Sh8d	10	37	0.53	4.21	57	240	0.75	372	5.3	7.1±0.4
04Sh8e	33	123	2.32	7.27	63	343	0.78	684	6.9	8.9±0.5
04Sh8f	65	289	3.69	3.80	54	240	0.74	962	5.1	6.9±0.4
04Sh8g	71	333	8.4	3.65	51	257	0.73	938	9.9	13.5±0.8
04Sh9Aa	20	106	8.8	3.16	51	223	0.72	343	32.6	44.6±2.7
04Sh9Ab	11	62	2.97	2.89	46	257	0.70	354	21.6	30.1±1.8
04Sh9Ac	2	5	0.53	3.91	57	223	0.75	169	33.9	41.3±2.5
04Sh9Ae	11	52	4.94	10.85	109	171	0.83	124	38.5	46.6±2.8
04Sh9Af	24	136	13.97	5.17	66	223	0.77	432	45.8	59.5±3.6
04Sh9Ag	17	88	3.12	5.11	57	291	0.75	218	15.2	20.2±1.2
04Sh10a	70	86	50.38	4.94	57	288	0.76	119	101.7	133.2±8.0
04Sh10b	42	76	23.71	7.16	72	257	0.80	130	72.0	90.2±5.4
04Sh10c	68	107	33.23	2.43	44	238	0.70	119	65.4	93.4±5.6
04Sh10d	76	104	43.34	12.38	76	403	0.82	152	78.8	96±5.8
04Sh13a	19	54	2.91	11.24	50	279	0.73	91	65.3	89.1±5.3
04Sh13b	28	108	3.81	23.35	37	250	0.65	294	79.3	121.1±7.3
04Sh13c	76	310	4.7	77.82	35	239	0.64	531	95.2	148.8±8.9
04Sh13d	17	67	4.5	12.43	42	189	0.67	160	69.9	103.6±6.2

[a] Corrected for alpha-ejection after Farley et al. (1996). Errors on single replicate analyses are 6% (2σ) and represent uncertainty on reproducibility of laboratory standards (Farley, 2002).

[b] Denotes replicates excluded from mean age calculated in Table 1 because of excess He compared to other replicated with similar U, Th, and Sm values.

References

Alam, M., Alam, M.M., Curray, J.R., Chowdhury, M.L.R., Gani, M.R., 2003. An overview of the sedimentary geology of the Bengal Basin in relation to the regional tectonic framework and basin-fill history. Sediment. Geol. 155, 179–208.

Allmendinger, R.W., Ramos, V.A., Jordan, T., Palma, M., Isacks, B.L., 1983. Paleogeography and Andean structural geometry, northwest Argentina. Tectonics 2 (604), 1–16.

Q1 An, Z., Kutzback, J.E., Prell, W.L., Porter, S.C., Evolution of Asian monsoons and phased uplift of the Himalayas–Tibet plateau since late Miocene times, Nature 411.

Anders, A.M., Roe, G.H., Hallet, B., Montgomery, D.R., Finnegan, N.J., Putkonen, J., 2006. Spatial patterns of precipitation and topography in the Himalaya. Geol. Soc. Am. Special Paper 398, 39–53.

Banerji, R.K., 1981. Cretaceous–Eocene sedimentation, tectonism and biofacies in the Bengal Basin, India. Palaeogeogr. Palaeoclimetol. Palaeoecol. 34, 57–85.

Banerji, R.K., 1984. Post-Eocene biofacies, paleoenvironments and paleogeography of the Bengal Basin, India. Palaeogeogr. Palaeoclimetol. Palaeoecol. 45, 49–73.

Bendick, R., Biham, R., 2001. How perfect is the Himalayan arc? Geology 29 (9), 791–794.

Q2 Biham, R., Comment on 'Interpreting the style of faulting and paleoseismicity associated with the 1897 Shillong, northeast India, earthquake' by C.P. Rajendran et al., Tectonics 25.

Biham, R., England, P., 2001. Plateau 'pop-up' in the great 1897 Assam earthquake. Nature 410, 806–809.

Biham, R., Bendick, R., Wallace, K., 2003. Flexure of the Indian Plate and intraplate earthquakes. Proc. Indian Acad. Sci. (Earth Planet Sci.) 112, 1–14.

Bilham, R., Larson, K.M., Freymueller, J.T., Jouanne, F., Le Fort, P., Leturmy, P., Mugnier, J.L., Gamond, J.F., Glot, J.P., Martinod, J., Chaudury, N.L., Chitrakar, G.R., Gautam, U.P., Koirala, B.P., Pandey, M.R., Ranabhat, R., Sapkota, S.N., Shrestha, P.L., Thakuri, M.C., Timilsina, U.R., Tiwari, D.R., Vidal, G., Vigny, C., Galy, A., de Voogd, B., 1997. GPS measurements of present-day convergence across the Nepal Himalaya. Nature 386 (6620), 61–64.

Bookhagen, B., T.R.C., S.M.R., 2005. Abnormal monsoon years and their control on erosion and sediment flux in the high, arid northwest Himalaya. Earth Planet. Sci. Lett. 231 (1–2), 131–146.

Brune, J., Singh, D.D., 1986. Continent-like crustal thickness beneath the bay of Bengal sediments. Bull. Seismol. Soc. Am. 76 (1), 191–203.

Catlos, E.J., Dubey, C.S., Harrison, T.M., Edwards, M.A., 2004. Late Miocene movement within the Himalayan Main Central Thrust shear zone, Sikkim, north-east India. J. Met. Pet. 22 (3), 207–226.

Chen, W.P., Molnar, P., 1990. Source parameters of earthquakes and intraplate deformation beneath the Shillong Plateau and the northern Indoburman ranges. J. Geophys. Res. 95 (8), 12,527–12,552.

Chowdhury, M.K.R. , Geological and Mineral map of Arunachal Pradesh, Assam, Manipur, Meghalaya, Mizoram, Nagaland and Tripura, 1:2,250,000 scale (1973).

Clark, M.K., Farley, K.A., in press (U-Th)/He analyses, various locations. Q3

Clark, M.K., House, M.A., Royden, L.H., Whipple, K.X., Burchfiel, B.C., Zhang, X., Tang, W., 2005. Late Cenozoic uplift of southeastern Tibet. Geology 33 (6), 525–528.

Coleman, M., Hodges, K., 1995. Evidence for Tibetan Plateau uplift before 14-Myr ago from a new minimum age for east–west extension. Nature 374 (6517), 49–52.

Cross, T.A., 1986. Tectonic controls of foreland basin subsidence and laramide style deformation, western United States. In: Allen, P.A., Homewood, P. (Eds.), Foreland Basins. Blackwell, Oxford, pp. 15–39.

Curray, J., Emmel, F., Moore, D., Raitt, R., 1982. Structure, tectonics and geological history of the northeastern Indian Ocean. In: Nairn, A., Stehli, F. (Eds.), The Ocean Basins and Margins. . The Indian Ocean, vol. 6. Plenum, New York, pp. 399–450.

Das Gupta, A.B., Evans, P., Metre, A.K., Visvanath, S.N., 1964. Tertiary geology and oilfields of Assam. In: Roy, B.C., Jhingran, A.G. (Eds.), International Geological Congress, 22nd session, New Delhi, India, p. 37.

Das Gupta, A.B., Biswas, A.K., 2000. Geology of Assam, Geological Society of India, Bangalore, India.

Dettman, D.L., Kohn, M.L., Quade, J., Ryerson, F.J., Ojha, T.P., Hamidullah, S., 2001. Seasonal stable isotope evidence for a strong Asian monsoon throughout the past 10.7 m.y. Geology 29, 31–34.

Ehlers, T.A., Farley, K.A., 2003. Apatite (U-Th)/he thermochronometry: methods and applications to problems in tectonics and surface processes. Earth Planet. Sci. Lett. 206 (1–2), 1–14.

Evans, P., 1932. Tertiary succession Assam. Trans. Min. Geol. Inst. India 27, 155–260.

Evans, P., 1964. The tectonic framework of Assam. J. Geol. Soc. India 5, 80–96.

Farley, K., 2000. Helium diffusion from apatite: general behavior as illustrated by Durango fluorapatite. J. Geophys. Res. 105, 2903–2914.

Farley, K., Rusmore, M.E., Bogue, S.W., 2001. Post 10-ma uplift and exhumation of the northern coast mountains, British Columbia. Geology 29, 99–102.

Farley, K., 2002. (U-Th)/He dating: techniques, calibrations, and applications. Rev. Mineral. Geochem. 47, 819–844.

Farley, K., Wolf, R.W., Silver, L.T., 1996. The effects of long-stopping distances on(U-Th)/He ages. Geochim. Cosmochim. Acta 60, 4223–4229.

Fitzgerald, P.G., Sorkhabi, R.B., Redfield, T.F., S.E., 1995. Uplift and denudation of the central Alaska range: a case study in the use of apatite fission track thermochronology to determine absolute uplift parameters. J. Geophys. Res. 100, 20,175–20,191.

Flint, J.J., 1974. Stream gradient as a function of order, magnitude, and discharge. Water Resour. Res. 10 (5), 969–973.

Gansser, A., 1983. Geology of the Bhutan Himalaya. Memoires de la Societe Helvetiques des Sciences Naturelles, vol. 96.

Ghosh, S., Fallick, A.E., Paul, D.K., Potts, P.J., 2005. Geochemistry and origin of Neoproterozoic granitoids of Meghalaya, northeast India; implications for linkage with amalgamation of Gondwana supercontinent. Gondwana Res. 8 (3), 421–432.

Grujic, D., Coutand, I., Bookhagen, B., Bonnet, S., Blythe, A., Duncan, C., 2006. Climatic forcing of erosion, landscape, and tectonics in the Bhutan Himalayas. Geology 34 (10), 801–804.

Hiller, K., Elahi, M., 1984. Structural development and hydrocarbon entrapment in the Surma Basin/Bangladesh (northwest Indo Burman fold belt). Proc. Offshore South East Asia (SEAPEX) Conf., vol. 5, pp. 6–50–6–63.

Hollister, L.S., Grujic, D., 2006. Pulsed channel flow in Bhutan. In: Law, R., Searle, M. (Eds.), Channel flow, ductile extrusion and exhumation of lower mid-crust in continental collision zones. Special Publication, vol. 268. Geological Society of London, pp. 415–423.

House, M.A., Farley, K.A., K.B.P., 1999. An empirical test of helium diffusion in apatite: borehole data from the Otway basin, Australia. Earth Planet. Sci. Lett. 170, 463–474.

House, M.A., Farley, K.A., Stockli, D., 2000. Helium thermochronometry of apatite and titanite using Nd-YAG laser heating. Earth Planet. Sci. Lett. 183, 365–368.

India, G.S., 2002. Geodynamic Atlas of India, Calcutta.

Jade, S., Bhatt, B.C., Yang, Z., Bendick, R., Gaur, V.K., Molnar, P., Anand, M.B., Kumar, D., 2004. GPS measurements from the Ladakh Himalaya, India; preliminary tests of plate-like or continuous deformation in Tibet. Geol. Soc. Am. Bull. 116 (11–12), 1385–1391.

Johnson, S.Y., Alam, A.M.N., 1991. Sedimentation and tectonics of the Sylhet Trough, Bangladesh. Geol. Soc. Am. Bull. 103 (11), 1513–1527.

Kayal, J.R., Arefiev, S.S., Barua, S., Hazarika, D., Gogoi, N., Kumar, A., Chowdhury, S.N., Kalita, S., 2006. Shillong plateau earthquakes in northeast India region: complex tectonic model. Curr. Sci. India 91, 109–114.

Kirby, E., Whipple, K.X., Tang, W., Chen, Z., 2003. Distribution of active rock uplift along the eastern margin of the Tibetan Plateau; inferences from bedrock channel longitudinal profiles. J. Geophys. Res. 108 (4), 24.

Kirby, E., Reiners, P.W., Krol, M.A., Hodges, K.V., Whipple, K.X., Farley, K.A., Chen, Z., Tang, W., 2002. Late Cenozoic evolution of the eastern margin of the Tibetan Plateau: inferences from ^{40}Ar/^{39}Ar and (U-Th)/He thermochronology. Tectonics 21, 1001.

Kroon, D., Steens, T., Troelstra, S.R., 1991. Onset of monsoonal related upwelling in the western Arabian sea as revealed by planktonic foramifers. Proceedings of the Ocean Drilling Project. Sci. Results, vol. 117. Ocean Drilling Program, College Station, Texas, pp. 257–263.

Lave, J., Avouac, J.P., 2000. Active folding of fluvial terraces across the Siwaliks Hills, Himalayas of central Nepal. J. Geophys. Res. 105 (3), 5735–5770.

Mathur, L.P., Evans, P., 1964. Oil in India. International Geological Congress, 22nd session, India, p. 87.

Mitchell, A.H.G., 1993. Cretaceous–Cenozoic tectonic events in the western Myanmar (Burma)–Assam region. J. Geol. Soc. London 150 (Part 6), 1089–1102.

Mitra, S., Priestley, K., Bhattacharyya, A.K., Gaur, V.K., 2005. Crustal structure and earthquake focal depths beneath Northeastern India and southern Tibet. Geophys. J. Intl. 160 (1), 227–248.

Molnar, P., England, P., 1990. Surface uplift, uplift of rocks, and exhumation of rocks. Geology 18 (12), 1173–1177.

Moore, M.A., E.P.C., 2001. On the inference of denudation rates from cooling ages of minerals. Earth Planet. Sci. Lett. 185 (3–4), 265–284.

Narr, W., Suppe, J., 1994. Kinematics of basement-involved compressive structures. Am. J. Sci. 294 (7), 802–860.

Niemi, N., Oskin, M., 2004. Utilizing stream power to derive uplift rates on active, blind structures. Southern California Earthquake Center Annual Meeting, p. 140.

Oldham, T., 1854. On the geological structure of part of the Khasi Hills, with observations on the meteorology and ethnology of that district, 4°. Geol. Surv. India, Calcutta. Q4

Oldham, R.D., 1899. Report on the great earthquake of 12th June, 1897. Mem. Geol. Surv. India 29, 379.

Pan, Y., Kidd, W.S.F., 1992. Nyainqentanglha shear zone; a late Miocene extensional detachment in the southern Tibetan Plateau. Geology 20 (9), 775–778.

Parrish, R.R., 1983. Cenozoic thermal evolution and tectonics of the coast mountains of British Columbia 1. fission-track dating, apparent uplift rates, and patterns of uplift. Tectonics 2, 601–631.

Prell, W.L., Murray, D.W., Clemens, S.C., Anderson, D.M., 1992. Evolution and variability of the Indian ocean summer monsoon: evidence from the western Arabian Sea drilling program. In: Duncan, R.A., Rea, D.K., Kidd, R.B., von Rad, U., Weissel, J.K. (Eds.), Synthesis of Results from Scientific Drilling in the Indian Ocean, American Geophysical Union, Washington D.C., pp. 447–469.

Rahman, M.J.J., Faupl, P., 2003. ^{40}Ar/^{39}Ar multigrain dating of detrital white mica of sandstones of the Surma Group in the Sylhet Trough, Bengal Basin, Bangladesh. Sediment. Geol. 155 (3–4), 383–392.

Rajendran, C.P., Rajendran, K., Duarah, B.P., Baruah, S., Earnest, A., 2004. Interpreting the style of faulting and paleoseismicity associated with the 1897 Shillong, northeast India, earthquake; implications for regional tectonism. Tectonics 23 (4), 12.

Rao Ranga, A., 1983. Geology and hydrocarbon potential of a part of Assam–Arakan Basin and its adjacent region. Pet. Asia J. 6, 127–158.

Reimann, K.U., 1993. Geology of Bangladesh. G. Borntraeger, Berlin.

Reiners, P.W., Brandon, M.T., 2006. Using thermochronology to understand orogenic erosion. Annu. Rev. Earth Planet. Sci. 34, 419–466.

Robinson, D.M., 2006. Exhumation of Greater Himalayan rock along the Main Central Thrust, Nepal: implications for channel flow. In: Law, R., Searle, M. (Eds.), Channel flow, ductile extrusion and exhumation of lower mid-crust in continental collision zones. Special Publication, vol. 268. Geological Society of London, pp. 865–885.

Rowley, D.B., 1996. Age of initiation of collision between India and Asia; a review of stratigraphic data. Earth Planet. Sci. Lett. 145 (1–4), 1–13.

Salt, C.A., Alam, M.M., Hossain, M.M., 1986. Bengal Basin: current exploration of the hinge zone area of southwestern Bangladesh. Proc. 6th Offshore Southeast Asia Conference, Singapore, pp. 55–57.

Schuster, D.L., F.R.M., F.K.A., 2006. The influence of natural radiation damage on helium diffusion kinetics in apatite. Earth Planet. Sci. Lett. 249 (3–4), 148–161.

Seeber, L., Armbruster, J., 1981. Great detachment earthquakes along the Himalayan arc and long-term forecasting. In: Simpson, D.W., Richards, P.G. (Eds.), Earthquake Prediction: An International Review. Maurice Ewing Series, vol. 4. AGU, Washington, D. C., pp. 259–277.

Seeber, L., Gornitz, V., 1983. River profiles along the Himalayan arc as indicators of active tectonics. Tectonophysics 92, 335–467.

Srinivasan, V., 2005. The Dauki Fault in northeast India; through remote sensing. J. Geol. Soc. India 66 (4), 413–426.

Uddin, A., Lundberg, N., 1998a. Cenozoic history of the Himalayan–Bengal system; sand composition in the Bengal Basin, Bangladesh. Geol. Soc. Am. Bull. 110 (4), 497–511.

Uddin, A., Lundberg, N., 1998b. Unroofing history of the eastern Himalaya and the Indo-Burman ranges; heavy-mineral study of Cenozoic sediments from the Bengal Basin, Bangladesh. J. Sediment. Res. 68 (3), 465–472.

Uddin, A., Lundberg, N., 2004. Miocene sedimentation and subsidence during continent–continent collision, Bengal Basin, Bangladesh. Sediment. Geol. 164 (1–2), 131–146.

Verma, R.K., Mukhopadhyay, M., 1977. An analysis of the gravity field in northeastern India. Tectonophysics 42 (2–4), 283–317.

W.A.B., 2001. Isostasy and flexure of the lithosphere. Cambridge University Press, Cambridge.

Wagner, G.A., Reimer, G.M., 1972. Fission-track tectonics: the tectonic interpretation of fission track ages. Earth planet. Sci. Lett. 14, 263–268.

Wagner, G.A., Reimer, G.M., J.E., 1977. Cooling ages derived by apatite fission track, mica Rb–Sr, Adn K–Ar dating: the uplift and cooling history of the central alps. Mem. Inst. Geol. Mineral. Univ. Padova 30, 1–27.

Wang, E., Burchfiel, B.C., Royden, L.H., Chen, L., Chen, J., Li, W., Chen, Z., 1998. Late Cenozoic Xianshuihe–Xiaojiang, Red River, Dali fault systems of southwestern Sichuan and central Yunnan, China. Geological Society of America Special Paper vol. 327.

Williams, H., Turner, S., Kelley, S.P., Harris, N.B.W., 2001. Age and composition of dikes in southern Tibet; new constraints on the timing of east–west extension and its relationship to postcollisional volcanism. Geology 29 (4), 339–342.

Wobus, C., Heimsath, A., Whipple, K., Hodges, K., 2005. Active out-of-sequence thrust faulting in the central Nepalese Himalaya. Nature 434 (7036), 1008–1011.

Worm, H.U., Ahmed, A.M.M., Ahmed, N.U., Islam, H.O., Huq, M.M., Hambach, U., Lietz, J., 1998. Large sedimentation rate in the Bengal Delta; magnetostratigraphic dating of Cenozoic sediments from northeastern Bangladesh. Geology 26 (6), 487–490.

Please cite this article as: Clark, M.K., Bilham, R., Miocene rise of the Shillong Plateau and the beginning of the end for the Eastern Himalaya, Earth Planet. Sci. Lett. (2008), doi:10.1016/j.epsl.2008.01.045